

A Numerically Accessible, High Precision Approximation of Landau Damping in Real Space

M. Pelkner, K. Hallatschek, M. Raeth

March 31, 2025

Abstract

Linear Landau damping tests of plasma codes are limited to density decay rate comparisons between approximations to the correct decay rate, obtained from the dielectric function, and simulated data. In this paper, we present a surprisingly simple numerical method for calculating the exact solution of the linearised Vlasov equation in the time domain, which allows for direct testing of simulated data. Specifically, when applied to the conventional evaluation of decay rates, the precision of our method is not restricted by any approximation. In addition, the method enables testing the complete distribution function as simulated by kinetic plasma codes. For illustration, we calculate the density and distribution function response to an initial density perturbation.

1 Overview

The spectrum of small-amplitude electron waves in collisionless, unmagnetised, fixed-ion background plasmas is, e.g., according to Goldston [1], determined by the zeros of the plasma dielectric function,

$$1 + \frac{e^2}{m_e k \epsilon_0} \int_{-\infty}^{\infty} dv \frac{\partial_v f_0}{\omega - kv} = 0, \quad (1)$$

and contains both damped and undamped modes [2], [3], [4], [5]. The damped spectrum originates from the infinitely many poles of the dielectric function (1) in the lower complex half plane, meaning that any wave within the damped spectrum can be understood as a superposition of infinitely many, damped plane waves with damping rates that are determined by the position of the corresponding complex pole. However, it is not possible to analytically Fourier invert this superposition. As a consequence, conventional Landau damping tests of plasma codes approximate the analytically correct mode by the slowest decaying plane wave of the superposition, or, in other words, by the complex pole with smallest imaginary part (fig. 1), [6], [7]. In this paper, the problematic analytic Fourier inversion is circumvented by numerically approximating the Fourier inversion integral using a simple and efficient method. Consequently, the precision of the standard density damping test (fig. 1), conducted with the proposed method in real space, is not limited by an approximation of the analytic decay rate. Furthermore, as will be explained subsequently, the method enables direct testing of complete

linear distribution function simulations. Both applications will be illustrated by an explicit calculation of the time evolution of the density and the time evolution of the distribution function for an initial density perturbation.

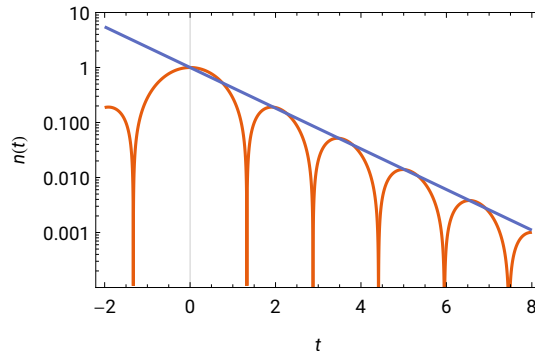


Figure 1: A standard Landau damping plot. The gradient of the straight line represents the damping of the most weakly damped plane wave of the superposition, as determined from pole with the smallest imaginary part of the dielectric function. For values of $t > 1$, the damping of the numerical simulation and the calculated damping rate approximately coincide, due to the fact that faster decaying contributions are already sufficiently damped. All data for this plot were calculated in Mathematica using the numerical method described in this paper.

2 Analytic solution in Fourier space

We assume the absence of magnetic fields ($B = 0$), quasi-neutrality ($n_e \approx n_i$) and, in contrast to the derivation by Landau [3], adiabatic electrons ($m_e \rightarrow 0$). At the end of this paper it will be argued why these assumptions do not restrict the applicability of the method to other scenarios. Restricting to one spatial dimension, the ion distribution function is first divided into a stationary part $f_0(v)$ and a small perturbation $f_1(x, v, t)$,

$$f(x, v, t) = f_0(v) + f_1(x, v, t). \quad (2)$$

The time evolution, or "response", of the distribution function is then determined by the linearised Vlasov equation,

$$\partial_t f_1 + v \partial_x f_1 - \frac{q}{m} \partial_x \phi \partial_v f_0 = 0, \quad (3)$$

where q denotes the ion charge and m denotes the ion mass [1]. Due to quasi-neutrality and adiabaticity, the electric potential is given by

$$\phi(x, t) = \frac{T}{qn_0} \int dv f_1(x, v, t), \quad (4)$$

where T is the temperature and n_0 is the constant particle density of the stationary background [8]. ϕ is of perturbation order. To simplify the notation and enhance its clarity, we will use the convention

$$g(\omega) = \int_{-\infty}^{\infty} \frac{dt}{\sqrt{2\pi}} g(t) e^{i\omega t} \quad (5)$$

and indicate the Fourier transform $g(\omega)$ of a function $g(t)$ only by changing the argument t to ω . We have taken care to avoid any potential confusion that may arise from this ambiguous definition. Furthermore, in order to facilitate the subsequent discussion of the numerical method, we have opted against working with the Laplace transform. Nevertheless, the following derivation is equivalent to the standard derivation documented in the literature [1]. In order to construct a solution f_1 of the homogeneous linear Vlasov equation (3) that satisfies a given initial condition $f_1(x, v, t = 0)$ at $t = 0$, we introduce

$$f_1^+(x, v, t) = \theta(t)f_1(x, v, t). \quad (6)$$

For positive times $t > 0$, the time evolution of f_1^+ is equivalent to the time evolution of the homogeneous solution f_1 . However, f_1^+ is not a solution of the homogeneous linear Vlasov equation (3), but of the inhomogeneous equation

$$\partial_t f_1^+ + v\partial_x f_1^+ - \frac{q}{m}\partial_x \phi \partial_v f_0 = f_1(x, v, t = 0)\delta(t), \quad (7)$$

which can be deduced by inserting f_1^+ into (3) and transforming to the frequency domain using (5). This provides the frequency domain equivalent of (7),

$$-i\omega f_1^+(x, v, \omega) + v\partial_x f_1^+(x, v, \omega) - \frac{q}{m}\partial_x \phi(x, \omega)\partial_v f_0 = \frac{1}{\sqrt{2\pi}}f_1(x, v, t = 0). \quad (8)$$

Accordingly, in order to calculate the time evolution of the homogeneous solution f_1 for positive times $t > 0$, equation (8) must first be solved for f_1^+ and then transformed back to the time domain. For the sake of simplicity, we consider an initial pure density perturbation

$$f_1(x, v, t = 0) = f_M(v)e^{ikx} \quad (9)$$

and postpone the discussion of how to deal with arbitrary initial perturbations. In this scenario, equation (8) is solved by a plane-wave ansatz for f_1^+ ,

$$f_1^+(x, v, \omega) = f_1^+(v, \omega)e^{ikx}, \quad (10)$$

which also imposes a plane-wave ansatz on ϕ by equation (4),

$$\phi(x, \omega) = \frac{T}{qn_0} \int dv f_1^+(v, \omega)e^{ikx} \equiv \frac{T}{qn_0} n_1^+(\omega)e^{ikx}. \quad (11)$$

We stress that, according to the convention that has been adopted, $\phi(x, \omega)$ is simply the Fourier transform of $\phi(x, t)$. Furthermore, since $f_1^+(x, v, t)$ and $f_1^+(v, t)$ are equivalent up to a multiplicative exponential, we refrain from introducing a different function name for $f_1^+(v, \omega)$. Plugging the plane-wave ansatz (10) into equation (8) and assuming a thermal background distribution, $f_0 = n_0 f_M$, we obtain

$$-i\omega f_1^+(v, \omega) + ikv f_1^+(v, \omega) + ikvn_1^+(\omega)f_M(v) = \frac{1}{\sqrt{2\pi}}f_M(v). \quad (12)$$

It is possible to eliminate the factors kv from equation (12) by redefining $kv \rightarrow v'$, which demonstrates that the solutions of equation (12) are similar for different values of k . Therefore, the solution for an arbitrary k can be deduced from the $k = 1$ solution by rescaling $v' \rightarrow v/k$. Selecting $k = 1$, equation (12) is solved by

$$f_1^+(v, \omega) = \text{p.v.} \left[\frac{1}{\omega - v} \left(v f_M(v) n_1^+(\omega) + \frac{1}{\sqrt{2\pi}} f_M(v) \right) \right] + a \delta(\omega - v), \quad (13)$$

where "p.v." denotes the Cauchy principal value and a is an arbitrary constant determined by the initial condition [9]. Due to pragmatic considerations, we employ the alternative yet equivalent definition of f_1 as the limit of a sequence of distributions [9],

$$f_1^+(v, t) = \lim_{\epsilon \rightarrow 0} \int \frac{d\omega}{\sqrt{2\pi}} f_{1,\epsilon}^+(v, \omega) e^{-i\omega t}, \quad (14)$$

where $f_{1,\epsilon}^+$ is defined by

$$f_{1,\epsilon}^+(v, \omega) = \frac{1}{\omega - v + i\epsilon} v f_M(v) n_{1,\epsilon}^+(\omega) + \frac{1}{\sqrt{2\pi}} \frac{i}{\omega - v + i\epsilon} f_M(v). \quad (15)$$

One of the benefits of this approach is that the undetermined constant a of equation (13) will emerge automatically without additional effort. To proceed, the density response $n_{1,\epsilon}^+$ is calculated from equation (15) by integrating over the velocity,

$$n_{1,\epsilon}^+(\omega) = -n_{1,\epsilon}^+(\omega) \int_{-\infty}^{\infty} dv \frac{v f_M(v)}{v - (\omega + i\epsilon)} - \frac{i}{\sqrt{2\pi}} \int_{-\infty}^{\infty} dv \frac{f_M(v)}{v - (\omega + i\epsilon)}. \quad (16)$$

Following the literature, we express the velocity integrals of equation (16) in terms of the plasma dispersion function with complex argument ζ [10],

$$Z(\zeta) = i\sqrt{\pi} e^{-\zeta^2} - 2D(\zeta) \quad D(\zeta) = e^{-\zeta^2} \int_0^{\zeta} e^{t^2} dt. \quad (17)$$

The plasma dispersion function is an entire function [11] and has been the subject of extensive numerical study [12]. Figure (2) illustrates the Dawson function $D(\zeta)$ along the real line.

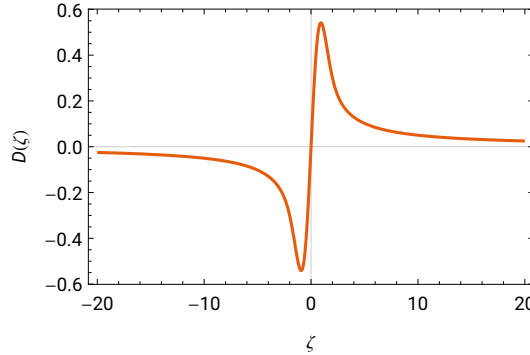


Figure 2: The Dawson function along the real line. For all values $\zeta \in \mathbb{C}$, $D(\zeta)$ is entire, antisymmetric and asymptotically proportional to $1/\zeta$.

Before proceeding, it is useful to normalise the time unit to the $k = 1$ ion sound wave frequency, $\omega_{\text{isw}}^2 = T/m = 1$, which in return defines

$$\zeta \equiv \frac{\omega}{\sqrt{2}}. \quad (18)$$

Using this normalisation, the final solution n_1^+ is calculated from $n_{1,\epsilon}^+$ according to definition (14). Since the plasma dispersion function is entire, the limit $\epsilon \rightarrow 0$ evaluates to

$$n_1^+(\omega) = -\frac{i}{2\sqrt{\pi}} \frac{Z(\zeta)}{2 + \zeta Z(\zeta)}. \quad (19)$$

With (19), f_1^+ is fully determined.

3 Density Landau damping

To calculate the time evolution of the density response (19), we numerically integrate the Fourier inversion

$$n_1^+(t) = -\frac{i}{2\sqrt{\pi}} \int_{-\infty}^{\infty} \frac{d\omega}{\sqrt{2\pi}} \frac{Z(\zeta)}{2 + \zeta Z(\zeta)} e^{-i\omega t}. \quad (20)$$

The integrand of (20) is free of singularities, since $Z(\zeta)$ is entire and the roots of $2 + Z(\zeta)$ are in the lower complex half-plane (fig. 3). As will become clear later, the convergence properties of our method are independent of the chosen numerical integration scheme. Any standard scheme documented in the literature, e.g. [13], will suffice. However, all integration schemes have the common feature of truncating the integration domain. As demonstrated in the figure 5, this truncation introduces inaccurate Gibbs oscillations, which are purely a numerical artefact and do not represent a physical phenomenon.

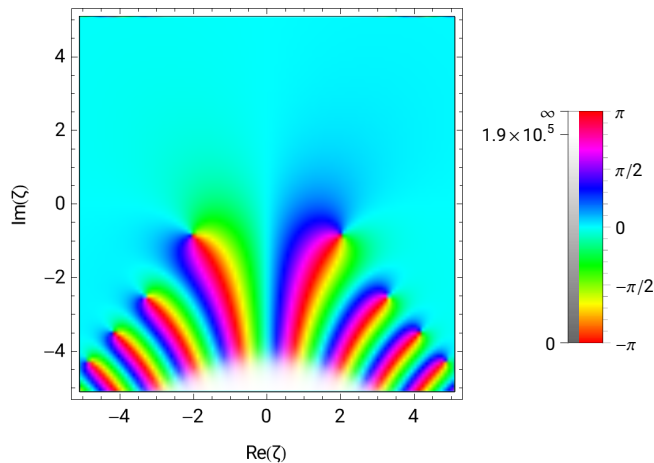


Figure 3: Complex plot of $2 + \zeta Z(\zeta)$. Roots are indicated by points around which closed paths pass once through all the colours of the rainbow. The aforementioned decomposition of (Landau-) damped modes into an infinite superposition of damped modes is obtained by pushing the integration contour of the Fourier inversion (20) down the imaginary axis.

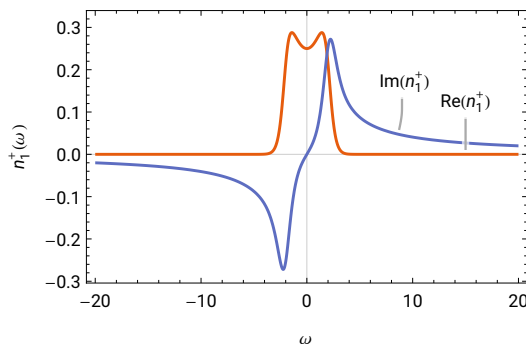


Figure 4: Fourier spectrum of the density response $n_1^+(\omega)$. The slowly decaying imaginary coefficients are the cause of Gibbs oscillations.

The origin of these oscillations can be understood by decomposing the density response n_1^+ into its real and imaginary components,

$$n_1^+(\omega) = \frac{2e^{-\zeta^2}}{\pi\zeta^2 e^{-2\zeta^2} + 4(1 - \zeta D(\zeta))^2} + \frac{i}{\sqrt{\pi}} \frac{-\pi\zeta e^{-2\zeta^2} + 4D(\zeta)(1 - \zeta D(\zeta))}{\pi\zeta^2 e^{-2\zeta^2} + 4(1 - \zeta D(\zeta))^2}, \quad (21)$$

using definition (17). While the real part of the spectrum decays like a Gaussian, the imaginary part decays $\propto \zeta^{-1}$ (fig. 4). It follows that, depending on the desired level of accuracy and the chosen numerical integration scheme, a large integration domain is required to achieve convergence of the Fourier integral (20). A domain of insufficient size will result in poor convergence and Gibbs oscillations. The origin of the problematic spectrum can intuitively be attributed to the discontinuity of f_1^+ at $t = 0$, since the Fourier transform of a step function

$$\int_{-\infty}^{\infty} \frac{dt}{\sqrt{2\pi}} e^{i\omega t} \theta(t) = \text{p.v.} \left(\frac{i}{\sqrt{2\pi\omega}} \right) + \sqrt{\frac{\pi}{2}} \delta(\omega), \quad (22)$$

decays $\propto \omega^{-1}$ [9]. Consequently, the Gibbs oscillations should be eliminated by removing the discontinuity from f_1^+ . At this stage there are numerous ad hoc methods conceivable to achieve this, the simplest of which seems to be the symmetrization of f_1^+ in time, as this requires no additional effort. As will be discussed in the subsequent section, symmetrization is actually the correct option in the sense of our numerical method, as it effectively transforms the inhomogeneous solution f_1^+ into the homogeneous solution f_1 . Symmetrizing the density response $n_1^+(t)$ in time is equivalent to symmetrizing $n_1^+(\omega)$ in the frequency domain, resulting in

$$n_1^{sym}(\omega) = \frac{2e^{-\zeta^2}}{\pi\zeta^2 e^{-2\zeta^2} + 4(1 - \zeta D(\zeta))^2}. \quad (23)$$

The spectrum (23) is real and decays like a Gaussian in ω . Due to this extremely fast decay, a small integration domain is sufficient to achieve high accuracy of the numerical solution. For example, since $\zeta = \omega/\sqrt{2}$, the coefficients outside $\omega \in [-8.5, 8.5]$ have already decayed to $O(10^{-16})$. Consequently, depending on the details of the numerical integration, a smaller interval can be selected to achieve machine precision. To illustrate the efficiency of our approach, we have numerically integrated

$$n_1^{sym}(t) = 2 \int_0^a \frac{d\omega}{\sqrt{2\pi}} n_1^{sym}(\omega) \cos(\omega t) \quad (24)$$

for $a = 4$ (fig. 6). The symmetrized solution n_1^{sym} describes a situation where a complicated perturbation of the distribution function at $t = -\infty$ evolves into a density perturbation at $t = 0$, fixed by the initial condition. Subsequently, due to symmetry in time, the density perturbation dissolves as a consequence of phase mixing (fig. 6).

4 Time Evolution of the Complete Solution

The previously outlined method is now approached more formally by considering the complete distribution function response. Although we still assume adiabatic electrons, $B = 0$, quasi-neutrality and a pure initial density perturbation (9), the following discussion already hints towards a generalisation of the method to arbitrary scenarios. Similar to f_1^+ (6), we define

$$f_1^-(x, v, t) = \theta(-t) f_1(x, v, t), \quad (25)$$

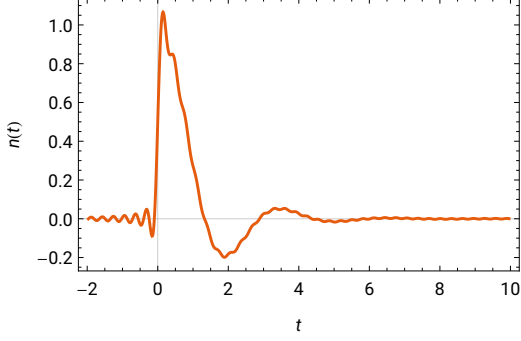


Figure 5: Plot of the Fourier inversion of the unsymmetrized density response n_1^+ with numerical integration domain $[-20, 20]$. At $t = 0$, the solution converges to exactly half of the correct value.

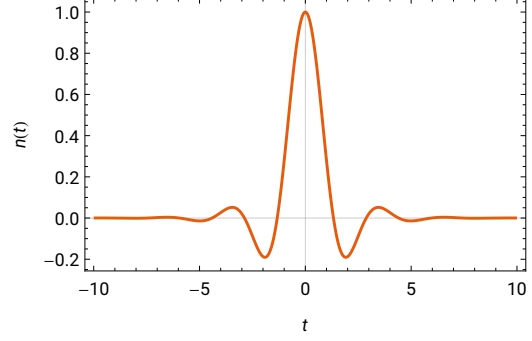


Figure 6: Plot of the Fourier inversion of the symmetrized density response n_1^{sym} with numerical integration domain $[0, 4]$. The symmetrization ensures a correct reconstruction of the initial condition at $t = 0$.

which solves the inhomogeneous linear Vlasov equation

$$\partial_t f_1^- + v \partial_x f_1^- - \frac{q}{m} \partial_x \phi \partial_v f_0 = -f_1(x, v, t = 0) \delta(t), \quad (26)$$

or, as before, its frequency domain equivalent

$$-i\omega f_1^-(x, v, \omega) + v \partial_x f_1^-(x, v, \omega) - \frac{q}{m} \partial_x \phi(x, \omega) \partial_v f_0(v) = -\frac{1}{\sqrt{2\pi}} f_1(x, v, t = 0). \quad (27)$$

Combining equations (6) and (25) decomposes any homogeneous solution f_1 of the linear Vlasov equation into a sum of two inhomogeneous solutions,

$$f_1(x, v, t) = f_1^+(x, v, t) + f_1^-(x, v, t). \quad (28)$$

In other words, adding f_1^+ and f_1^- removes the inhomogeneities in the frequency domain. If the homogeneous solution f_1 is smooth, it can be shown that its Fourier spectrum decays at least faster than any polynomial, which is sufficient for the Fourier inversion to be computationally efficient [14]. Therefore, we first construct f_1 via (28) and then evaluate the Fourier inversion numerically. In the special case of a time-symmetric initial condition, such as the previously considered initial density perturbation, it can be seen that

$$f_1^-(v, \omega) = f_1^+(-v, -\omega) \quad (29)$$

by time inverting the defining differential equation of f_1^+ (8), which affects both time and velocity, and comparing to (27). Therefore, in this particular instance, f_1 can be constructed by symmetrizing f_1^+ in time or, equivalently, in the frequency. Doing so for $f_{1,\epsilon}$ yields

$$f_{1,\epsilon}^{sym}(v, \omega) = \frac{\omega - v}{(\omega - v)^2 + \epsilon^2} v f_M(v) n_1^{sym}(\omega) + \frac{\epsilon}{(\omega - v)^2 + \epsilon^2} \left(\sqrt{\frac{\pi}{2}} f_M(v) - i v f_M(v) n_1^{asym}(\omega) \right), \quad (30)$$

where $n_1^{\text{asym}}(\omega) = n_1^+(\omega) - n_1^+(-\omega)$. From equation (30) and the definition of the distributional sequence (14) it is evident that the homogeneous solution f_1 consists of a principal value integral and two integrals involving delta functions. The Fourier inversion of the delta contributions can be approached analytically, yet the principal value integral with integrand

$$g(v, \omega) = \frac{\omega - v}{(\omega - v)^2 + \epsilon^2} v f_M(v) n_1^{\text{sym}}(\omega) \quad (31)$$

must be Fourier inverted numerically. The spectrum of g decays like a Gaussian due to the factor n_1^{sym} , but the real singularity in the limit $\epsilon \rightarrow 0$ is problematic.

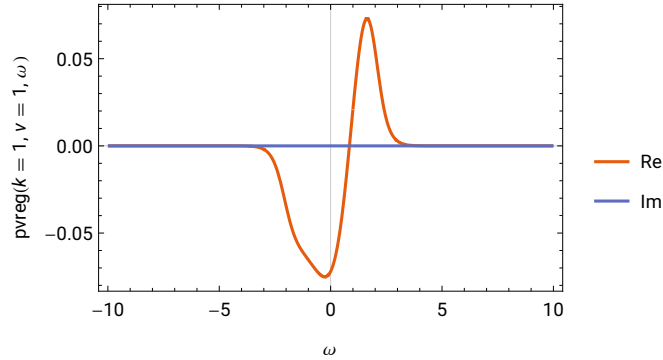


Figure 7: Illustration of the regularised principle value spectrum (33).

To avoid numerical integration over this pole, the following technique is applied: first, the singularity is subtracted from g ; then, the obtained regularised principal integrand g_{reg} is integrated numerically; and finally, the subtracted singularity is Fourier transformed analytically and added to the numerical integration. We begin by introducing

$$c(v) = \left(g(v, \omega) \Big|_{\epsilon=0} (\omega - v) \right) \Big|_{\omega=v} = v f_M(v) n_1^{\text{sym}}(v) \quad (32)$$

and defining the regularised principal value integrand (fig. 7),

$$g_{\text{reg}}(v, \omega) = g(v, \omega) \Big|_{\epsilon=0} - c(v) \frac{e^{-(\omega-v)^2}}{\omega - v}. \quad (33)$$

The exponential factor in (33) is required to not introduce a slow decay proportional to $\propto \omega^{-1}$ into the spectrum by subtracting the singularity. The Fourier inversion of the subtracted pole,

$$p(v, \omega) = c(v) \frac{e^{-(v-\omega)^2}}{\omega - v}, \quad (34)$$

is calculated analytically to [9]

$$p(v, t) = -ic(v) \sqrt{\frac{\pi}{2}} \operatorname{erf}\left(\frac{t}{2}\right) e^{-ivt} \quad \operatorname{erf}(\zeta) = \frac{2}{\sqrt{\pi}} \int_0^\zeta e^{-t^2} dt \quad \zeta \in \mathbb{C}. \quad (35)$$

In total, the time evolution the distribution function response is given by

$$f_1(v, t) = \int_{-a}^a \frac{d\omega}{\sqrt{2\pi}} g_{\text{reg}}(v, \omega) e^{-i\omega t} + p(v, t) + f_M(v) \left(1 - iv \sqrt{\frac{\pi}{2}} n_1^{\text{asym}}(v) \right) e^{-ivt}. \quad (36)$$

As in the preceding section, due to the Gaussian decay of g_{reg} , a small integration domain suffices to achieve machine precision of the numerical integration. The physical implications of equation (36) have been illustrated in several plots. For a fixed time, all terms in equation (36) are suppressed by at least a Gaussian factor in the velocity. As a result, the perturbation f_1 becomes arbitrarily small for large velocities at any time (fig. 8). Conversely, in order to consider a fixed velocity, it is beneficial to decompose the perturbation f_1 into an adiabatic contribution and a non-adiabatic perturbation h ,

$$f_1(x, v, t) = h(x, v, t) - \frac{qn_0}{T} \phi(x, t) f_0(v). \quad (37)$$

Assuming adiabatic electrons, the time evolution of the non-adiabatic perturbation h is described by the inhomogeneous equation

$$\partial_t h + v \partial_x h = f_0 \partial_t n_1. \quad (38)$$

A general solution of (38) consists of a homogeneous and an inhomogeneous contribution, $h = h_{\text{hom}} + h_{\text{part}}$, where the homogeneous solution h_{hom} solves

$$\partial_t h + v \partial_x h = 0. \quad (39)$$

It can be deduced from the preceding discussion that, for large times, $\partial_t n \rightarrow 0$. Consequently, only the homogeneous contribution h_{hom} persists in this limit. Therefore, at a constant velocity, f_1 evolves within a characteristic time from a perturbed state to the free streaming solution (fig. 9).

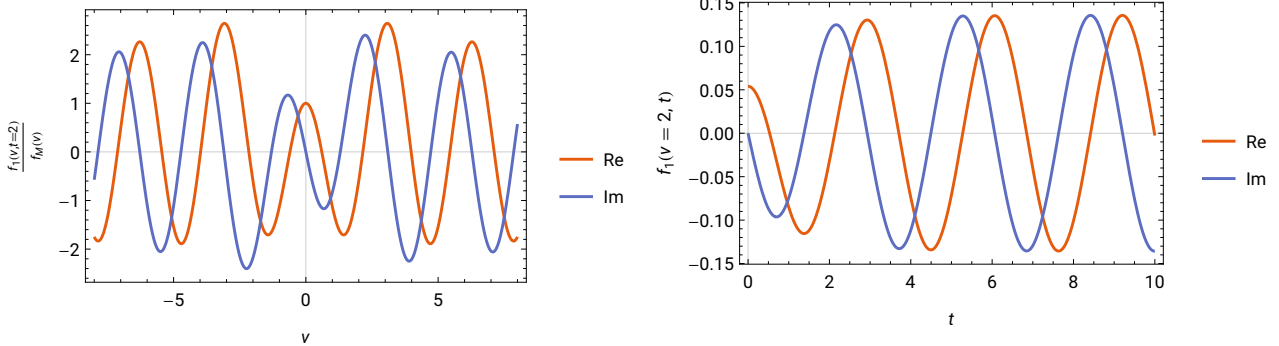


Figure 8: Plot of f_1 at a fixed time, normalised by a Maxwellian in order to remove the Gaussian suppression in v . In accordance with expectations, due to symmetry in time, the real part is symmetric in v .

Figure 9: Plot at a fixed velocity. The distribution function transitions from a perturbed state with amplitude modulations to the free-streaming solution. The modulations are caused by perturbations of the electric potential ϕ .

Since the homogeneous solution f_1 is complex, the asymptotics of both the absolute value of f_1 and its complex argument are of interest. Following our previous reasoning, the particular solution h_{part} can be immediately identified as

$$h_{\text{part}}(v, t) = \lim_{\epsilon \rightarrow 0} \int \frac{d\omega}{\sqrt{2\pi}} \frac{\omega}{\omega - v + i\epsilon} n_1^{\text{sym}} f_M(v) e^{-i\omega t}. \quad (40)$$

Furthermore, since $f_1 = h_{\text{part}} - n_1 f_M + h_{\text{hom}}$ (37), the combination of terms

$$\int_{-\infty}^{\infty} \frac{d\omega}{\sqrt{2\pi}} g_{\text{reg}}(v, \omega) e^{-i\omega t} + p(v, t) \quad (41)$$

in the defining equation of f_1 (36) is equivalent to the difference $h_{\text{part}} - n_1 f_M$. The pole (35) resulting from this difference contributes to the overall homogeneous solution h_{hom} .

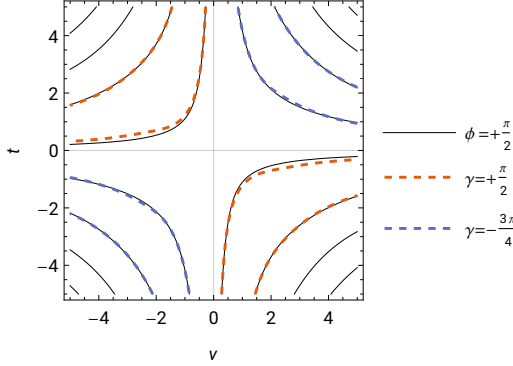


Figure 10: A contour plot in the $t - v$ plane. The black lines represent lines of constant complex argument ϕ of the distribution function response f_1 . The dashed red and blue lines represent lines of constant γ , which by construction asymptotically approximates ϕ . It can be seen that the contours of ϕ and γ coincide for $|t > 1|$.

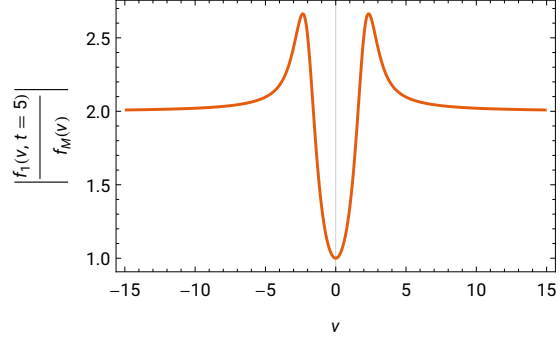


Figure 11: Plot of the absolute value of f_1 at a constant time, normalised by a Maxwellian. The time has been chosen sufficiently late so that all Landau damped terms have already vanished.

The asymptotic value of the homogeneous solution f_1 at a fixed time is plotted ideally normalised by a Maxwellian and after all Landau damped terms have vanished, which is equivalent to plotting

$$\left| p(v, t) + f_M(v) \left(1 - iv \sqrt{\frac{\pi}{2}} n_1^{\text{asym}}(v) \right) e^{-ivt} \right| f_M^{-1}(v), \quad (42)$$

assuming $\text{erf}(t) = 1$ (fig. 11). The asymptotics of the complex phase are treated analogously by plotting

$$\gamma \equiv \arg \left[p(v, t) + f_M(v) \left(1 - iv \sqrt{\frac{\pi}{2}} n_1^{\text{asym}}(v) \right) e^{-ivt} \right], \quad (43)$$

again assuming $\text{erf}(t) = 1$. For further illustration, the normalised absolute value of f_1 has been plotted in two three-dimensional plots, along with the complex phase (fig. 12), (fig. 13). To summarize, we have constructed an initial state of f_1 at $t = -\infty$ that forces the ions to transfer half of their free energy to the adiabatic electrons until $t = 0$, where both species share the same amount of free energy. Thereafter, the electrons transfer all of their free energy back to the ions. As the entire process unfolds at a minimum of free energy, the density perturbation at $t = 0$ is a consequence of phase mixing, arising from a complex reversible motion of the distribution function.

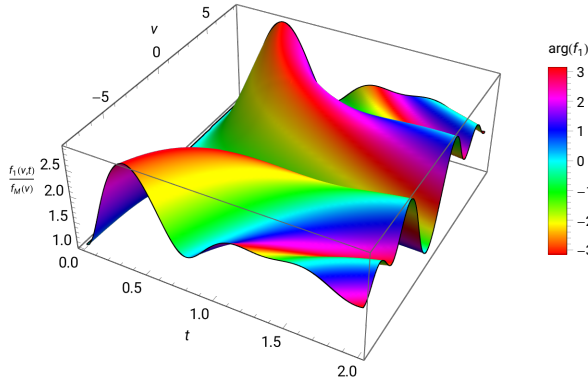


Figure 12: Plot of the normalised absolute value of f_1 for $t \geq 0$. The values of the complex argument are indicated by a rainbow colour function, which allows to identify the previously plotted lines of constant complex argument.

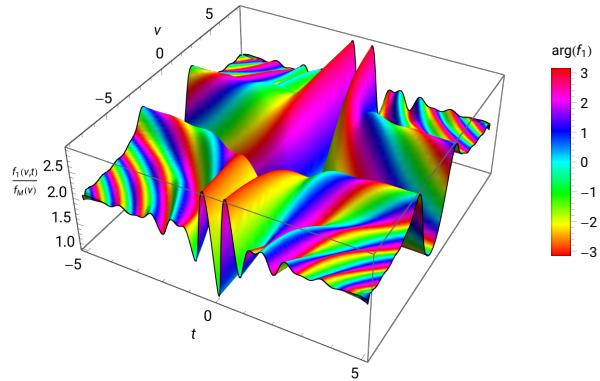


Figure 13: A plot analogous to (fig. 12), but for a more substantial and time symmetric section of the $t - v$ space.

5 Generalization

The initial step in constructing a numerically well-behaved distribution function response for an arbitrary perturbation $f_1(x, v, t = 0)$ at $t = 0$ was to separate the homogeneous solution f_1 into two inhomogeneous solutions f_1^+ and f_1^- (28). One approach to construct the homogeneous solution f_1 involves calculating both solutions f_1^+ and f_1^- by solving (8) and (27), respectively. The alternative approach, as outlined in this paper, constructs f_1 from either f_1^+ or f_1^- by exploiting the time inversion symmetry of the linear Vlasov equation (3). By construction, the inhomogeneous solutions (6) and (25) are not time symmetric, which is reflected by the presence of the inhomogeneities in (8) and (27). However, the homogeneous part of the inhomogeneous equations (7) and (26) is time symmetric. This allows to cancel the inhomogeneities in both solutions f_1^+ and f_1^- by symmetrizing according to the symmetry properties of the initial perturbation $f_1(x, v, t = 0)$, which has been demonstrated for a time-symmetric, initial pure density perturbation. In this particular instance, we showed that the homogeneous solution f_1 can be constructed by time-symmetrizing the solution f_1^+ ; similarly, an antisymmetrization of f_1^+ would be required for a time-antisymmetric initial condition. Consequently, an arbitrary initial condition without specific symmetry can be addressed by first decomposing it into a symmetric and an antisymmetric part, and then symmetrizing each component individually. This procedure is equally applicable to arbitrary scenarios described by the Vlasov-Maxwell system, since Maxwell's equations are time-symmetric. Therefore, a numerically well-behaved distribution function response can always be constructed by eliminating the inhomogeneities from either f_1^+ or f_1^- , which is solely a matter of the symmetry properties of the initial perturbation.

6 Conclusion

We have presented a general numerical scheme to compute the time evolution of the linearised Vlasov-Maxwell system after applying an arbitrary perturbation at $t = 0$. The method has been demonstrated by calculating the response of the density and the distribution function to an initial pure density perturbation. Our primary use case is to test the performance of our code BSL6D in linear Landau damping scenarios. In addition to evaluating the performance in density Landau damping (6), we have refined the testing process to assess the time evolution of the full distribution function as demonstrated in figure 14. However, many other applications of the method to linear plasma physics processes are conceivable.

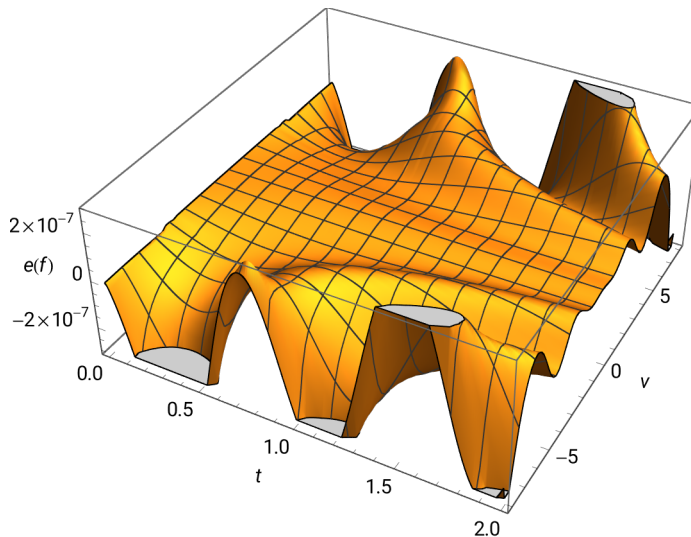


Figure 14: Illustration of the relative error $e(f)$ of a BSL6D distribution function simulation. BSL6D is a semi-Lagrange, full Vlasov ion code with adiabatic electrons that employs a Strang splitting in time and Lagrange interpolation in space to update distribution function values at discrete grid points by back-tracing the characteristics in phase space [6], [15]. For the above plot, a 1D1V simulation with 32×65 points on a domain $[0, 2\pi] \times [-8, 8]$ was performed for the time interval $[0, 2]$ with $dt = 0.01$, using an eight point stencil for the Lagrange interpolation. In BSL6D, time is measured in inverse ion gyrofrequencies. The relative error of the simulation increases towards the edges of the velocity domain since the Lagrange interpolation error depends on the particles' shift. For higher velocities, the shift is larger for a given time step, resulting in a greater interpolation error.

7 Acknowledgments

This work has been carried out partly within the framework of the EUROfusion Consortium, funded by the European Union via the Euratom Research and Training Programme (Grant Agreement No 101052200 – EUROfusion). Support has also been received by the EUROfusion High Performance Computer (Marconi-Fusion). Views and opinions expressed are however those of the author(s) only and do not necessarily reflect those of the European Union or the European Commission. Neither the European Union nor the European Commission can be held responsible for them. Numerical simulations were performed at the MARCONI-Fusion

supercomputer at CINECA, Italy, and at the HPC system at the Max Planck Computing and Data Facility (MPCDF), Germany.

References

- [1] Goldston R. J; Rutherford P. H. *Introduction to plasma physics*. Taylor & Francis Groups, 2019.
- [2] A Vlasov. On the kinetic theory of an assembly of particles with collective interaction. *Russ. Phys. J.*, 9:25–40, 1945.
- [3] L. D. Landau. On the vibrations of the electronic plasma. *J. Phys. (USSR)*, 10:25–34, 1946.
- [4] K.M Case. Plasma oscillations. *Annals of Physics*, 7(3):349–364, 1959.
- [5] N.G. Van Kampen. On the theory of stationary waves in plasmas. *Physica*, 21(6):949–963, 1955.
- [6] K. Kormann, K. Reuter, and M. Rampp. A massively parallel semi-lagrangian solver for the six-dimensional vlasov–poisson equation. *The International Journal of High Performance Computing Applications*, 33:924–947, 2019.
- [7] D. Finn, M. Knepley, J. Puszta, and M. Adams. A numerical study of landau damping with petsc-pic. *Communications in Applied Mathematics and Computer Science*, 18:135–152, 2023.
- [8] G Knorr and J Nuehrenberg. The adiabatic electron plasma and its equation of state. *Plasma Physics*, 12(12):927, 1970.
- [9] Ram P. Kanwal. *Generalized Functions : Theory and Applications*. Birkhäuser Boston, 2004.
- [10] A.S. Richardson, United States. Office of Naval Research, and Naval Research Laboratory (U.S.). *2019 NRL Plasma Formulary*. Naval Research Laboratory, 2019.
- [11] B.D. Fried and S.D. Conte. *The Plasma Dispersion Function: The Hilbert Transform of the Gaussian*. Academic Press, 1961.
- [12] S. Wang and S. Huang. Evaluation of the numerical algorithms of the plasma dispersion function. *Journal of Quantitative Spectroscopy and Radiative Transfer*, 234:64–70, 2019.
- [13] J. Stoer, R. Bartels, W. Gautschi, R. Bulirsch, and C. Witzgall. *Introduction to Numerical Analysis*. Texts in Applied Mathematics. Springer New York, 2002.
- [14] E.M. Stein and R. Shakarchi. *Fourier Analysis: An Introduction*. Princeton lectures in analysis. Princeton University Press, 2011.
- [15] Nils Schild, Mario R ath, Sebastian Eibl, Klaus Hallatschek, and Katharina Kormann. A performance portable implementation of the semi-lagrangian algorithm in six dimensions. *Computer Physics Communications*, 295:108973, 2024.